A Study of the Effect of Model Resolution in Analysis of Building Thermal Dynamics

Ali Saberi Derakhtenjani[1], Andreas K. Athienitis[1]
[1]Department of Building, Civil and Environmental Engineering
Concordia University, Montreal, Quebec, Canada

Abstract

This paper presents a study of the effect of model resolution of thermal networks with different level of detail for a zone with a floor heating system. It is investigated how different model resolutions affect the floor heating load calculation. Also, the frequency response analysis of different building thermal network models is presented. A lumped parameter finite difference model is used to model an office building with radiant floor heating system. It is investigated how different assumptions applied in such a model affect the floor heating load calculation. Then, derivation of the floor admittance transfer functions (for 1-D heat transfer) is presented (for the exact theoretical solution as well as the RC model estimation). The admittance transfer functions of the lower order RC models are compared with the ones obtained from the exact theoretical solution. It is demonstrated how an optimization technique can help in obtaining the effective RC circuits parameters to match the frequency response of the RC models transfer functions with the one from the theoretical solution. Finally, it is observed that for building materials with higher thermal mass, higher order models are needed so that to model a slab accurately while the low order RC circuit parameters make physical sense.

Introduction

Studying the dynamic thermal response of a building offers significant benefits in different aspects of building energy performance including operation of building energy management systems, design of building thermal systems and retrofit of existing buildings. It has been reported that accurate modeling of building thermal dynamics and proper functioning of the HVAC systems could save up to seventy-five percent of the required load (Haghighat et al. (1988)).

Building energy models are used as a tool to analyze buildings thermal dynamics and optimize building operation. Choosing the most suitable approach to create a building energy model is the vital step in developing the right model for a desired application. Every modeling techniques has its own specific advantages and shortcomings. Therefore, depending on the objective of a study, the most efficient approach should be considered. Here some of the recent and previous studies of two different energy modeling techniques (low-order RC models and frequency domain models) are briefly presented.

Simplified low-order models

When it comes to model building thermal dynamics to reproduce reality, usually a large amount of data is required which is not always feasible. Also, while many efforts can be made for the relatively heavy data processing, still many uncertainties exist for which an assumption is considered and nevertheless a certain level of model calibration is required. Reduced order models have much less parameters than the highly-detailed models and this is one of the major advantages of the low-order models. Having fewer parameters in a model will also facilitate setting up the initial conditions which is an important consideration in building thermal controls (Candanedo et al. (2013)). Also, less computational effort will be required. However, the challenge is developing a low-order model that represents the building thermal dynamics accurate enough for a desired objective.

Candanedo et al. (2013) proposed a methodology to create simplified RC models for the purpose of control studies (control-oriented modeling). Then, Candanedo et al. (2015) used the proposed methodology to develop the low-order grey-box RC models and studied different temperature setpoint strategies to find an optimum air temperature setpoint trajectory using the model. Saberi Derakhtenjani et al. (2015) created low-order models using experimental data for an environmental chamber. Bacher and Madsen (2011) proposed a procedure for model identification suited to different applications in building thermal studies. Fraisse et al. (2002) investigated low-order RC model for walls. Xu and Wang (2007) developed a low-order grey-box RC model for a commercial building. Rodríguez et al. (2016) proposed an approach based on adjusting the position of thermal capacitance to obtain a simplified first-order RC model of buildings. Kramer et al. (2012) published a review on simplified building models.

Frequency domain models

Frequency domain techniques have been shown to be a useful approach in the analysis of building thermal dynamics, especially in the early stages of building design or for building operation. Studying specific building transfer functions provides significant insight into building thermal dynamics and on relative performance of design options (Athienitis et al. (1990)). Saberi Derakhtenjani and Athienitis (2016) evaluated the effect of different design parameters on the building energy performance by studying the frequency domain transfer functions. Recent building energy and control studies

using frequency domain techniques include works by Chen et al. (2013a), Chen et al. (2013b) and Chen et al. (2014). Also, Wang and Xu (2006) performed an optimization routine on the frequency domain transfer functions to find a second-order RC model (2C3R) for building thermal mass. This work investigates the development of different low-order RC models and the effect of different model resolution in studying building thermal dynamics.

Description of the thermal zone

The thermal zone considered in this study is an office room as shown in Figure 1. The walls are gypsum board with RSI 4 insulation for each wall. The south facing façade has a 2m×3m window area (two thirds of the facade area). The floor is made of concrete and represents the main thermal mass in the zone. This test room has been built (with different types of auxiliary systems) at Concordia University for experiments at the solar simulator-environmental chamber (SSEC) laboratory of Concordia University. This study presents some simulations results performed for this thermal zone.

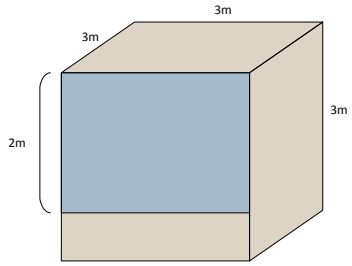

Figure 1. Office (thermal zone) geometry

Finite-difference model

Methodology

This section presents the lumped capacitance finite difference model for the thermal zone and the model application to calculate the auxiliary floor heating load. Floor as the main thermal mass in the room (10cm thick concrete), is modelled with different numbers of thermal capacitances (different level of detail). It is investigated how the level of detail in modeling the floor will affect the auxiliary heating load calculation.

The convective heat transfer coefficients are calculated using the following equations (ASHRAE (2005)):

For horizontal surfaces:

$$h_c = 1.52(|T_s - T_{air}|)^{1/3} \quad (1)$$

For vertical surfaces:

$$h_c = 1.31(|T_s - T_{air}|)^{1/3} \quad (2)$$

where T_s is surface temperature and T_{air} is air temperature in the room. The radiative heat transfer coefficients between the room surfaces are linearized and calculated as follows:

$$U_{ij} = A_i F_{ij}^{*} (4\sigma T_m^{3}) \quad (3)$$

where:

A_i = area of surface i,

$h_{c,i}$ = convective heat transfer coefficent of surface i,

F_{ij}^{*} = radiant exchange factor between surfaces i and j,

T_m = mean surfaces temperature

The auxiliary heating source is considered to be placed at the bottom of the slab. A proportional controller based on the difference between the air temperature and the air setpoint is used to calculate the auxiliary load:

$$Q_{aux} = K_p (T_{sp} - T_{air}) \quad (4)$$

K_p (the proportional constant=928W/K) is estimated using a technique presented by Athienitis (1994).

Figure 2 shows the thermal network for the finite difference model. One lumped capacitance is considered for each wall (made of gypsum board) to represent the thermal mass. Also, one lumped thermal capacitance (control volume) is considered to model the floor as the main thermal mass in the zone.

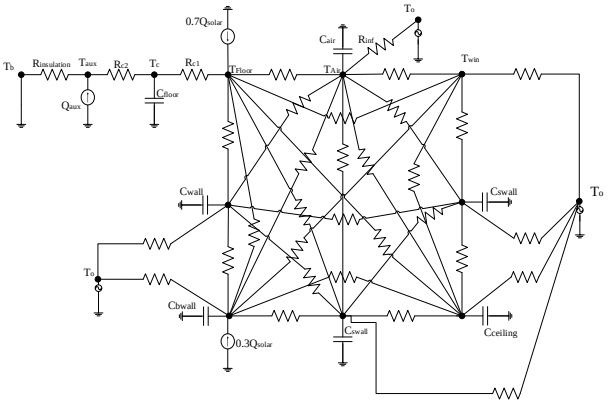

Figure 2. Thermal network for the finite difference model

in Figure 2, Rc1 and Rc2 represent the floor concrete R-value and each is equal to the half of the total thermal resistance of the concrete. Floor thermal capacitance is represented by C_{floor}. $R_{insulation}$ is the insulation layer under the floor concrete and T_b is the basement temperature. The auxiliary heating load is inserted at the node T_{aux} just underneath the concrete. The solar gain in the room is assumed to be a sinusoidal profile as shown in Figure 3. It is assumed that 70% of the solar gain is absorbed by the floor and the remaining thirty percent is absorbed by the back wall. The air setpoint temperature, T_{sp}, is considered to be constant and equal to 21ºC. The outdoor temperature is assumed to be constant and equal to -10 ºC.

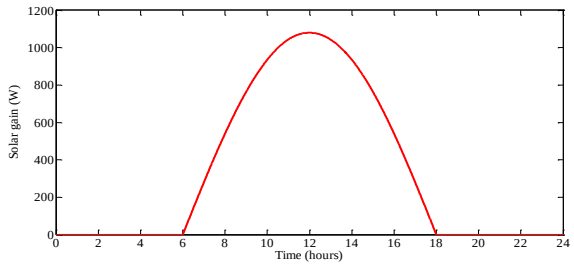

Figure 3. Solar gain profile for the time when solar radiation peak equals to 200W/m^2

Results

In the thermal network shown in Figure 2, the convective and radiative heat transfers are modelled separately and the respective coefficients change based on the temperature change of the room surfaces and air. This is a necessary modeling aspect to be considered while creating a model for the rooms with radiant heating systems or the rooms with high solar gains. Figure 4 shows that using the less detailed models with constant heat transfer coefficients and combined heat transfer coefficients, leads to significant overestimation of the required heating load for the room.

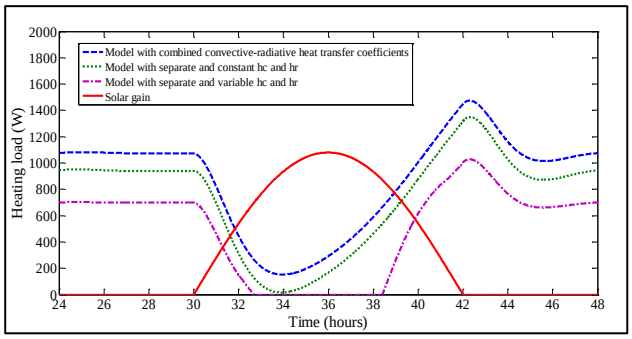

Figure 4. Heating load calculated with different modelling assumptions

The results are shown for the second day since the first day results are affected by the initial conditions. All the models used in Figure 4 consider a 1C2R model for the floor. The models are all basically the same and their only difference is in modeling of heat transfer coefficients.

Floor model with different level of detail: results and discussion

It is investigated how the number of discrete thermal capacitances considered to model the floor thermal mass affects the floor auxiliary load calculation. Figure 5 shows the 2C3R model thermal network for the floor. Each capacitance is half of the total floor capacitance and Rc1, Rc2 and Rc3 are one-third of the total concrete thermal resistance each.

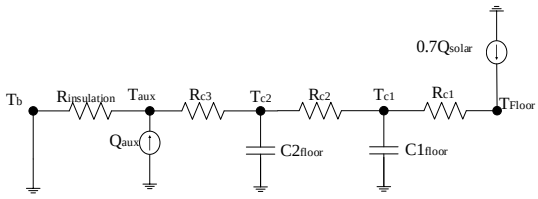

Figure 5. 2C3R thermal model network for floor

Two other models with more number of capacitances (four and six capacitances) are created as shown in Figure 6. The same process is done to create these models and the concrete capacitances and resistances are all equal to each other.

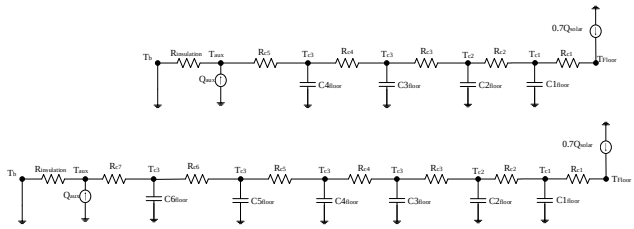

Figure 6. 4C5R model (top) and 6C7R (bottom) model thermal networks for floor

Figure 7 shows the calculated auxiliary load using different models. It is observed that there are some differences in the peak load estimation between different models. However, they all follow a general trend and generally there is negligible discrepancy between the plots from different models.

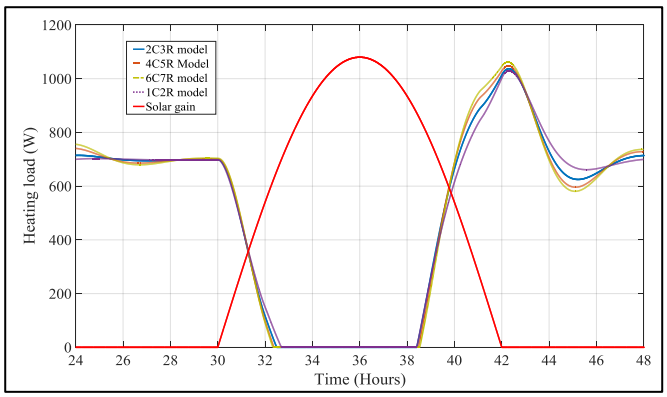

Figure 7. Floor auxiliary load calculated using floor models with different resolutions

Frequency-domain modelling

Methodology

This section presents the theoretical frequency characteristics of heat transfer through building surfaces.

The procedure to obtain the transmission matrix (also known as the cascade matrix) of heat transfer for one dimensional homogenous wall in Laplace domain has been described in many literatures [Davies (1973), Pipes (1957)]. Here it is presented as follows.

Consider a slab as shown in Figure 8 with two surfaces (exterior and interior) named surface 1 and 2.

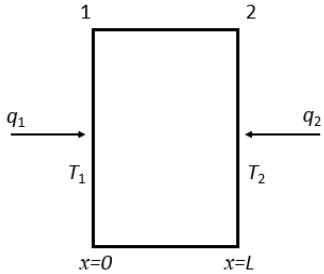

Figure 8. Slab with its two sides temperatures and heat sources

The 1-D Fourier conduction law is applied as follows:

$$\alpha \frac{\partial^2 T(x,t)}{\partial x^2} = \frac{\partial T(x,t)}{\partial t} \qquad (5)$$

Where α is thermal diffusivity and equals to: $k/\rho C_p$. Applying the Laplace transform to equation (5) assuming the initial condition $T(x,t=0)=0$, transforms the partial differential equation to an ordinary differential equation:

$$\alpha \frac{\partial^2 T(x,s)}{\partial x^2} = sT(x,s) \qquad (6)$$

for which the solution is obtained as:

$$T(x,s) = C_1 e^{\gamma x} + C_2 e^{-\gamma x} = M\cosh(\gamma x) + N\sinh(\gamma x) \qquad (7)$$

where $\gamma = \sqrt{s/\alpha}$. Then, for the heat flux we will have:

$$q = -k\frac{dT}{dx} \Rightarrow q(x,s) = -Mk\gamma\sinh(\gamma x) - Nk\gamma\cosh(\gamma x) \qquad (8)$$

Applying equations (7) and (8) to each surface gives:

$$\begin{cases} T_1 = T(x=0,s) = M \\ q_1 = q(x=0,s) = -Nk\gamma \\ T_2 = T(x=l,s) = M\cosh(\gamma l) + N\sinh(\gamma l) \\ q_2 = q(x=l,s) = Mk\gamma\sinh(\gamma l) + Nk\gamma\cosh(\gamma l) \end{cases}$$

or in the matrix form it can be written as:

$$\begin{bmatrix} T_2 \\ q_2 \end{bmatrix} = \underbrace{\begin{bmatrix} \cosh(\gamma l) & -\sinh(\gamma l)/k\gamma \\ k\gamma\sinh(\gamma l) & -\cosh(\gamma l) \end{bmatrix}}_{\text{TR}} \begin{bmatrix} T_1 \\ q_1 \end{bmatrix} \qquad (9)$$

in equation (9) , the matrix TR is the transmission matrix for the slab. Equation (9) is the exact theoretical solution for the one-dimensional heat transfer that relates the temperatures and heat fluxes on the two surfaces of the slab to each other.

Now by rearranging equation (9) we will have:

$$\begin{bmatrix} q_1 \\ q_2 \end{bmatrix} = \begin{bmatrix} k\gamma/\tanh(\gamma l) & -k\gamma/\sinh(\gamma l) \\ -k\gamma/\sinh(\gamma l) & k\gamma/\tanh(\gamma l) \end{bmatrix} \begin{bmatrix} T_1 \\ T_2 \end{bmatrix} \qquad (10)$$

and the respective admittance transfer functions are obtained as:

$$\text{(self-admittance)} \quad Y_{1,1} = \frac{q_1}{T_1} = \frac{k\gamma}{\tanh(\gamma l)} \quad (T_2 = 0)$$

$$\text{(Transfer-admittance)} \quad Y_{1,2} = \frac{q_1}{T_2} = \frac{-k\gamma}{\sinh(\gamma l)} \quad (T_1 = 0)$$

Actually if we consider the transmission matrix in equation (9) as:

$$\text{TR} = \begin{bmatrix} A & B \\ C & D \end{bmatrix}$$

Then it can be shown that:

$$Y_{1,1} = D/B \ , \ Y_{1,2} = (BC - AD)/B$$

In the case when there is negligible thermal mass (an insulation layer) the TR matrix for the layer will be equal to:

$$\begin{bmatrix} 1 & 1/u \\ 0 & 1 \end{bmatrix}$$

where u is the insulation u-value. Therefore, in the case where we have an insulation layer on the exterior surface of the slab, the transmission matrix will be:

$$\begin{bmatrix} \cosh(\gamma l) & \sinh(\gamma l)/k\gamma \\ k\gamma\sinh(\gamma l) & \cosh(\gamma l) \end{bmatrix} \begin{bmatrix} 1 & 1/u \\ 0 & 1 \end{bmatrix} \qquad (11)$$

Then, the admittance transfer functions will be obtained as:

$$Y_{1,1} = \frac{u + k\gamma\tanh(\gamma l)}{\frac{u}{k\gamma}\tanh(\gamma l) + 1} \quad , \quad Y_{1,2} = \frac{-1}{\frac{\cosh(\gamma l)}{u} + \frac{\sinh(\gamma l)}{k\gamma}}$$

Derivation of the transmission matrix for the lumped capacitance models

The slab shown in Figure 8 can be modeled using a number of lumped thermal capacitances. Here an approach is presented to obtain the transmission matrix for different lumped parameter models with different resolutions.

Initially, a first order model is considered for the slab as shown in Figure 9:

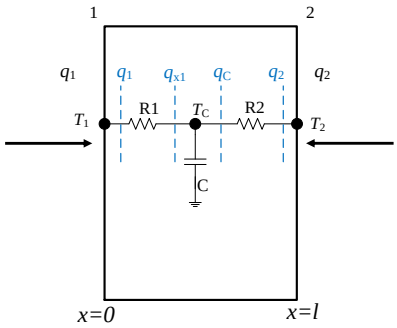

Figure 9. 1C2R model for the slab

The transmission matrix for this model can be obtained by writing the energy balance equation for the nodes T_1 and T_2 in Laplace domain considering all the heat fluxes and the intermediate node:

$$\begin{cases} q_1(t) = q_{x1}(t) \\ q_{x1}(t) = \dfrac{T_C(t) - T_1(t)}{R_1} \\ q_C(t) - q_{x1}(t) = C(dT_C(t)/dt) \end{cases} \qquad (12)$$

by applying the Laplace transform to equation (12) we will have:

$$\begin{cases} q_1(s) = q_{x1}(s) \\ q_{x1}(s) = \dfrac{T_C(s) - T_1(s)}{R_1} \\ q_C(s) = q_{x1}(s) + sCT_C(s) \quad (T_C(0) = 0) \end{cases} \qquad (13)$$

Now from equation (13) we can say:

$$\begin{cases} T_C(s) = T_1(s) + R_1 q_1(s) \\ q_C(s) = sCT_1(s) + q_1(1 + sCR_1) \end{cases} \Rightarrow$$

$$\begin{bmatrix} T_C \\ q_C \end{bmatrix} = \underbrace{\begin{bmatrix} 1 & R_1 \\ sC & 1+sCR_1 \end{bmatrix}}_{TR1} \begin{bmatrix} T_1 \\ q_1 \end{bmatrix} \quad (14)$$

TR1 is the transmission matrix between nodes T_C and T_1 and can be written as:

$$\begin{bmatrix} 1 & R_1 \\ sC & 1+sCR_1 \end{bmatrix} = \begin{bmatrix} 1 & 0 \\ sC & 1 \end{bmatrix} \begin{bmatrix} 1 & R_1 \\ 0 & 1 \end{bmatrix} \quad (15)$$

Then, writing the energy balance equations for the nodes T_C and T_2 (interior wall surface) gives:

$$\begin{cases} q_C(t) = q_2(t) \\ q_2(t) = \dfrac{T_2(t) - T_C(t)}{R_2} \end{cases} \xrightarrow{\text{Laplace transfrom}} \begin{cases} q_C(s) = q_2(s) \\ q_2(s) = \dfrac{T_2(s) - T_C(s)}{R_2} \end{cases}$$

and by rearranging the equations we will have:

$$\begin{cases} T_2(s) = T_C(s) + R_2 q_C(s) \\ q_2(s) = q_C(s) \end{cases} \Rightarrow \begin{bmatrix} T_2 \\ q_2 \end{bmatrix} = \underbrace{\begin{bmatrix} 1 & R_2 \\ 0 & 1 \end{bmatrix}}_{TR2} \begin{bmatrix} T_C \\ q_C \end{bmatrix} \quad (16)$$

where TR2 is the transmission matrix between T_C and T_2. Using equations (15) and (16) we will have:

$$\begin{bmatrix} T_2 \\ q_2 \end{bmatrix} = \overbrace{\underbrace{\begin{bmatrix} 1 & R_2 \\ 0 & 1 \end{bmatrix}}_{TR2} \begin{bmatrix} 1 & 0 \\ sC & 1 \end{bmatrix} \underbrace{\begin{bmatrix} 1 & R_1 \\ 0 & 1 \end{bmatrix}}_{TR1}}^{TRtot} \begin{bmatrix} T_1 \\ q_1 \end{bmatrix} \quad (17)$$

The matrix TRtot is the total transmission matrix between nodes T_1 and T_2. It can be observed from equation (17) that generally, the transmission matrix for every layer that contains only a thermal resistance, R, is written as:

$$\begin{bmatrix} 1 & R \\ 0 & 1 \end{bmatrix}$$

and for a layer that contains only thermal capacitance, C, is written as:

$$\begin{bmatrix} 1 & 0 \\ sC & 1 \end{bmatrix}$$

using this rule, the transmission matrix for higher order RC circuits can be obtained. Now, considering a second-order circuit (2C3R) for the slab as shown in Figure 10, the transmission matrix is formed as:

$$\begin{bmatrix} T_2 \\ q_2 \end{bmatrix} = \begin{bmatrix} 1 & R_3 \\ 0 & 1 \end{bmatrix} \begin{bmatrix} 1 & 0 \\ C_2 s & 1 \end{bmatrix} \begin{bmatrix} 1 & R_2 \\ 0 & 1 \end{bmatrix} \begin{bmatrix} 1 & 0 \\ C_1 s & 1 \end{bmatrix} \begin{bmatrix} 1 & R_1 \\ 0 & 1 \end{bmatrix} \begin{bmatrix} T_1 \\ q_1 \end{bmatrix}$$

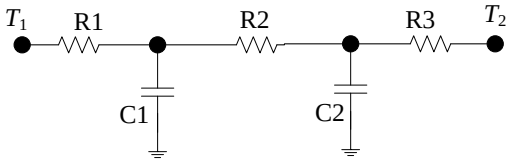

Figure 10. 2C3R model

In Figure 10 all the resistances are assumed each to be equal to the one-third of the total resistance (R_{tot}) and the capacitances are assumed each equal to the half of the total slab thermal capacitance. These assumptions are discussed in the next section. Also, the procedure to find the equivalent circuit parameters (resistances and capacitances) by means of optimization techniques is presented.

Results

Figure 11 compares the magnitude and phase angle of the transfer function $Y_{1,1}$ from the exact theoretical solution (no discretization) and different RC circuits approximation.

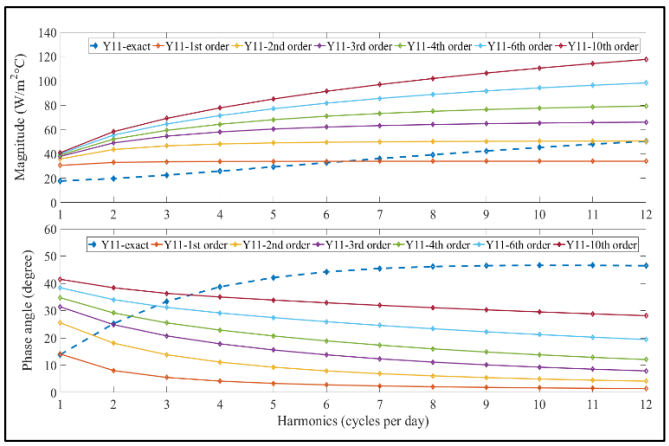

Figure 11. Magnitude and phase angle plot for transfer functions $Y_{1,1}$

It is observed that the RC circuit models act like a low-pass filters and pass signals up to a certain frequency (cut-off frequency) and attenuates higher frequency signals. This cut-off frequency increases as the model order is increased and after that the magnitude of the transfer function remains constant. Therefore, significant differences between the magnitude and phase angles of the exact model response and RC circuits models response were observed. Hence, an optimization routine is considered to find the effective RC circuit parameters (resistances and capacitances) that improve the match between the two models.

An objective function is defined as the second norm of the summation of the differences between the magnitude (M) and the phase angles (Ph) of the transfer functions with each having their respective weighting factor. $(YE)_n$ is the value of the theoretical self-admittance transfer function at frequency n and Ye is the self-admittance transfer function of the low-order RC circuit estimation.:

$$J = W_M \sqrt{\sum_n \left[M(YE)_n - M(Ye)_n \right]^2} + W_{PH} \sqrt{\sum_n \left[Ph(YE)_n - Ph(Ye)_n \right]^2} \quad (18)$$

The second norm is defined as:

$$\sqrt{\sum_j x_j^{\,2}} = \sqrt{x_1^{\,2} + x_2^{\,2} + \ldots + x_m^{\,2}}$$

The frequency range considered (1-12 cycles per day) is rational for majority of heat transfer phenomena that happen inside a building. The MATLAB optimization toolbox (fmincon function which uses the simplex algorithm) is used. Initially, it is decided to consider an equal weight for the magnitudes and the phase angles

differences (W_M=W_{PH}=*1*). Therefore, from equation (18) the objective function J_1 will be:

$$J_1 = \sqrt{\sum_n \left[M(YE)_n - M(Ye)_n\right]^2} + \sqrt{\sum_n \left[Ph(YE)_n - Ph(Ye)_n\right]^2} \quad (19)$$

Now considering the first-order (1C2R) model, Figure 12 shows the optimization results:

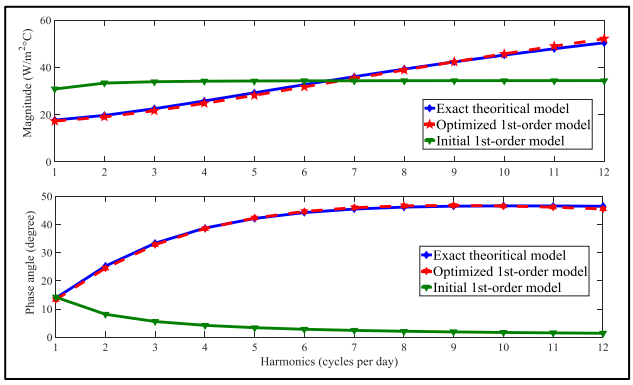

Figure 12. Comparison of the optimized first-order model with the theoretical model

It is observed from Figure 12 that the match has improved considerably both in terms of magnitudes and phase angles. However, let us verify the new circuit parameters obtained through optimization with the initially proposed values (based on physical properties of the slab materials). The parameters are shown in Table 1:

Table 1. First-order RC circuit parameters

Parameters	Initial values	Optimized values
C (J)	1.58E+06	7.71E+04
R1 (m^2K/W)	3.00E-02	5.07E-02
R2 (m^2K/W)	3.00E-02	9.43E-03
R1+R2	6.00E-02	6.01E-02

we can see that the thermal capacitance has been reduced significantly and in terms of the resistance distribution between R1 and R2, more than eighty percent of the total R-value has been given to R1. However, the total R-value which is the summation of the R1 and R2 is very close to the initial total R-value of the slab from the physical model. Nevertheless, the new thermal capacitance value does not make sense physically since it is less than five percent of the physical model. Thus, it is clear that higher order models should be considered.

Now, let us consider a second-order circuit (2C3R model). Figure 13 shows the optimization results for the second-order circuit. From Figure 13 we can see a very good match between the optimized second-order circuit and the theoretical model. Table 2 shows the RC circuit parameters. From Table 2, we can see that the optimized circuit total capacitance value has become closer to its initial total physical value (8.66E05/1.58E06 ≈55%) compared to the first-order model (7.71E04/1.58E06≈4%). For the resistances, the total resistance is almost the same for both the initial and optimized circuits. In the optimized circuit, the largest resistance is considered to be the middle resistance R2 (more than 75% of the total R) and R3 considered to be the smallest. Therefore, it can be observed that the initial assumption to consider all the thermal resistances to be the same is not the best approximation. It can also be seen that increasing the order of the model from first-order (1C2R) to second-order (2C3R) has improved the optimization results in a sense that the equivalent circuit parameters are closer to the physical values.

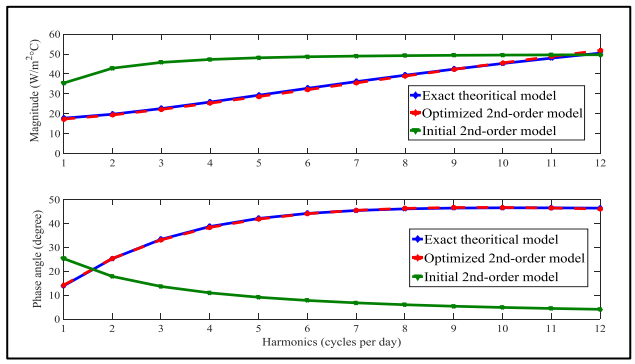

Figure 13. Comparison of the optimized second-order model with the theoretical model

Table 2.Second-order RC circuit parameters

Parameters	Initial values	Optimized
C1 (J)	7.92E+05	7.92E+05
C2 (J)	7.92E+05	7.40E+04
C1+C2 (total C)	1.58E+06	8.66E+05
R1 (m^2K/W)	2.00E-02	4.67E-03
R2 (m^2K/W)	2.00E-02	4.71E-02
R3 (m^2K/W)	2.00E-02	8.89E-03
R1+R2+R3	6.00E-02	6.06E-02

Considering the same procedure for a third-order model (3C4R), the results are shown in Figure 14 and Table 3.

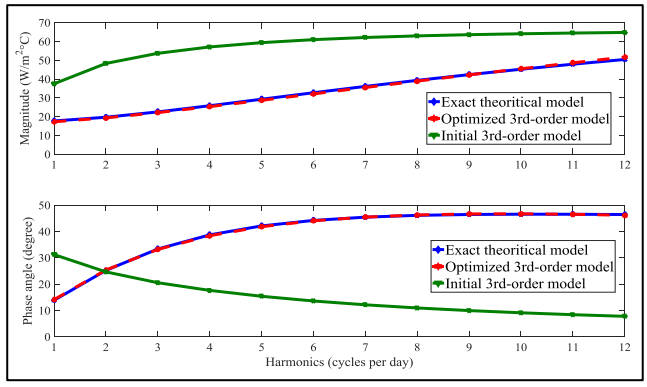

Figure 14. Comparison of the optimized Third-order model with the theoretical model

It is observed that for the third-order model the values of the capacitances C1 and C2 are identical before and after the optimization and the total value of the capacitances are closer to each other compared to the second-order model.

For the third-order model, the value of model's total capacitance after optimization is almost seventy-two percent of the total value considered in the initial physical model. Thus, it can be observed that by increasing the model order the results are getting closer to the initial model created based on the physical properties.

Table 3. Third-order RC circuit parameters

Parameters	Initial values	Optimized
C1 (J)	5.28E+05	5.28E+05
C2 (J)	5.28E+05	5.28E+05
C3 (J)	5.28E+05	7.30E+04
C1+C2+C3	1.58E+06	1.13E+06
R1 (m^2K/W)	1.50E-02	1.35E-05
R2 (m^2K/W)	1.50E-02	5.92E-03
R3 (m^2K/W)	1.50E-02	4.58E-02
R4 (m^2K/W)	1.50E-02	8.75E-03
R1+R2+R3+R4	6.00E-02	6.05E-02

The above procedure is also carried out for the gypsum board with the total thermal mass of 2.34E+04 (J) and it is observed that when the sixth-order model (6C7R) is considered, the total value of thermal capacitance is very close to the physical model; that is the difference is less than two percent. The results are shown in Table 4 and Figure 15:

Table 4.Sixth-order model for gypsum board

Parameters	Initial values	Optimized
C1 (J)	3.90E+03	3.91E+03
C2 (J)	3.90E+03	3.91E+03
C3 (J)	3.90E+03	3.90E+03
C4 (J)	3.90E+03	3.90E+03
C5 (J)	3.90E+03	3.88E+03
C6 (J)	3.90E+03	3.50E+03
ΣC	2.34E+04	2.30E+04
R1 (m^2K/W)	1.17E-02	1.42E-03
R2 (m^2K/W)	1.17E-02	1.66E-03
R3 (m^2K/W)	1.17E-02	1.82E-03
R4 (m^2K/W)	1.17E-02	2.05E-03
R5 (m^2K/W)	1.17E-02	3.23E-03
R6 (m^2K/W)	1.17E-02	5.83E-02
R7 (m^2K/W)	1.17E-02	1.27E-02
ΣR	8.20E-02	8.12E-02

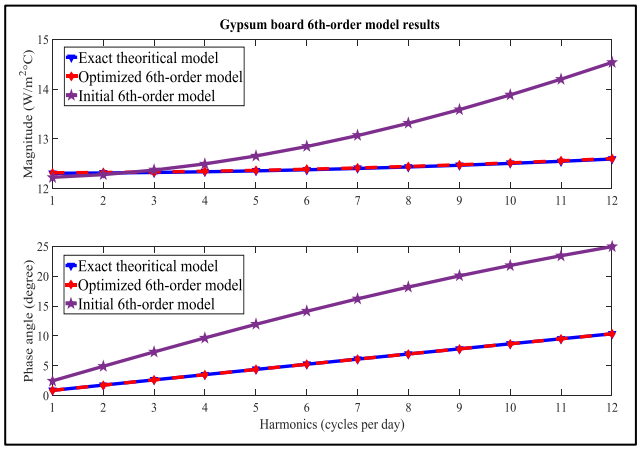

Figure 15.Comparison of gypsum board's 6th-order model

Thus, it can be seen that the smaller the amount of thermal mass, the lower number of the capacitances and resistances required to model the slab with a decent accuracy while also having a physically meaningful model parameters. If the 6C7R model is considered for the concrete, then the total thermal capacitance of the optimized model is about eighty-eight (88%) percent of the physical model. Therefore, higher order models are needed to increase the physical meaning of the optimized model parameters. Actually, simulation results shows that considering an eighth order model (8C9R) makes it closer (92%) to the total value compared to the sixth-order model. Another important observation in all those RC models is that we can see the optimization algorithm arranges the parameters in a way that the larger capacitances and smaller resistances are put in the beginning of the circuit (R1, R2…, C1, C2, …) and the smaller capacitances and larger resistances are placed towards the end of the circuit.

Objective function based on the magnitude difference only

The objective function considered in the previous simulations was introduced by equation (19) in which magnitudes and phase angles have the same weight and actually importance in the optimization problem. Now, here it is studied how the results will change if we consider a different objective function in which the weighting factor of the phase angles difference is put equal to zero as shown in equation (20) :

$$J_2 = \sqrt{\sum_n \left[M(YE)_n - M(Ye)_n \right]^2} \qquad (20)$$

Now considering this objective function, Table 5 and Figure 16 show the results for the third-order model of the concrete slab:

Table 5.Third-order circuit parameters using different objective functions

Parameters	Initial values	J_1	J_2
C1 (J)	5.28E+05	5.28E+05	5.28E+05
C2 (J)	5.28E+05	5.28E+05	5.28E+05
C3 (J)	5.28E+05	7.30E+04	8.54E+04
ΣC	1.58E+06	1.13E+06	1.14E+06
R1 (m^2K/W)	1.50E-02	1.35E-05	2.26E-05
R2 (m^2K/W)	1.50E-02	5.92E-03	3.55E-03
R3 (m^2K/W)	1.50E-02	4.58E-02	4.33E-02
R4 (m^2K/W)	1.50E-02	8.75E-03	1.20E-02
ΣR	6.00E-02	6.05E-02	5.89E-02

It is observed from Table 5 that the change in the total value of the thermal capacitances and resistances is not significant compared to the previous optimization results. Also, from Figure 16 it is observed that although the phase angles difference was removed from the objective function, the phase angle plot has improved noticeably compared to the initial model. Therefore, the important observation here is that the most important parameter is the magnitude of the transfer function over this frequency range.

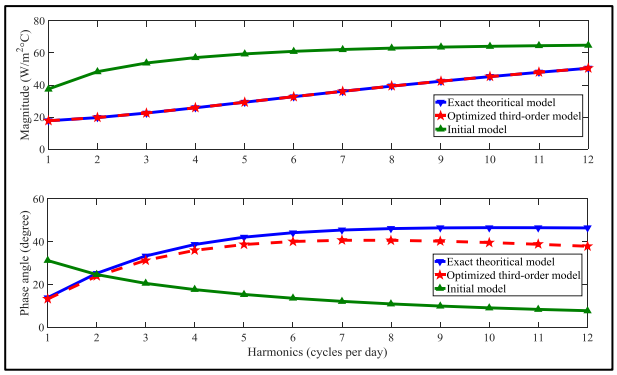

Figure 16. Comparison of the new third-order model for the concrete slab

Final remarks

It should be noted that in all the optimized different order models studied here, our main objective was to find a model that has the physically meaningful parameters otherwise, one can have a very good fit even by using a first-order model that has the physically meaningless parameters.

Conclusion

This paper presented a study of the effect of model resolution in analysis of thermal dynamics of building elements. By means of a lumped capacitance model it was investigated that simplified assumptions considered in modeling the heat transfer coefficients in a room with floor heating system lead to overestimation of the radiant floor heating load. Also, no significant difference is observed for calculating the floor heating load when the floor model order is increased. However, the results should be verified by means of experiment which is planned next in the current project.

The procedure to obtain the exact theoretical solution for a slab transfer functions (self-admittance and transfer admittance) is described. Then, a methodology is presented to find the cascade matrix for the low-order resistance capacitance (RC) models of a slab and the self-admittance transfer functions of the low-order RC models were compared with the ones from the exact theoretical solution.

Then, an optimization algorithm (simplex method) is used to find the equivalent RC circuit parameters to improve the match with the theoretical model. The first objective function considered to be the second norm of the difference between the magnitudes and the phase angles of the transfer functions with an equal weighting factor. It is discussed that for different low-order RC models if the optimized model parameters physically make sense compared to the initial physical model or not. It is observed that depending on the level of thermal mass, higher order models are needed to have a good match with the exact solution while having a physically meaningful model at the same time. Then, by removing the phase angles from the objective function, it is also observed that the most important parameter is the magnitude of a transfer function and considering only magnitudes differences in the optimization objective function improves the phase angles match to a certain degree too.

As the future work, a series of experiments will be performed to calibrate the developed models based on the zone admittance values and to verify simulation results. The methodology presented here to develop low-order models will be used in further thermal dynamic studies and control applications.

Acknowledgement

This work was perfromed under the NSERC/Hydro-Quebec industrial research chair held by professor Athienitis at Concordia University. The financial and technical support from the chair is greatly acknowledged.

References

ASHRAE (2005). *ASHRAE Handbook Fundamentals*. Atlanta, GA.

Athienitis, A.K. (1994). *Building thermal analysis*. Boston,MA, USA, MathSoft Inc.

Athienitis, A.K., Stylianou, M. and Shou, J. (1990). A methodology for building thermal dynamics studies and control applications. *ASHRAE Transactions* 96(2).

Bacher, P. and Madsen, H. (2011). Identifying suitable models for the heat dynamics of buildings. *Energy and Buildings* 43(7): 1511-1522.

Candanedo, J, Dehkordi, V, Saberi Derakhtenjani, A. and Athienitis , A. K. (2015). Near-optimal transition between temperature setpoints for peak load reduction in small buildings. *Energy and Buildings* 87: 123-133.

Candanedo, J., Dehkordi, V. and Lopez, Ph. (2013). A control-oriented simplified building modeling strategy. *IBPSA Chambery , France*.

Chen, Y., Athienitis , A. K. and Galal, Kh. (2013a). Frequency domain and finite difference modeling of ventilated concrete slabs and comparison with field measurements: Part 1, modeling methodology. *International Journal of Heat and Mass Transfer* 66: 948-956.

Chen, Y., Athienitis , A. K. and Galal, Kh. (2013b). Frequency domain and finite difference modeling of ventilated concrete slabs and comparison with field measurements: Part 2. Application. *International Journal of Heat and Mass Transfer* 66: 957-966.

Chen, Y., Athienitis , A. K. and Galal, Kh. (2014). A charging control strategy for active building-integrated thermal energy storage systems using frequency domain modeling. *Energy and Buildings* 84: 651-661.

Davies, M.G. (1973). The thermal admittance of layered walls. *Building Science* 8(3).

Fraisse, G., Viardot, C., Lafabrie, O. and Achard, G. (2002). Development of a simplified and accurate

building model based on electrical analogy. *Energy and Buildings* 34(10): 1017-1031.

Haghighat, F., Fazio, P. and Zmeureanu, R. (1988). A systematic approach for derivation of transfer function coefficients of buildings from experimental data *Energy and Buildings* 12(2): 101-111.

Kramer, R., Schijndel, J. V. and Schellen, H. (2012). Simplified thermal and hygric building models: A literature review. *Frontiers of Architectural Research* 1: 318-325.

Pipes, Louis A. (1957). Matrix analysis of heat transfer problems. *Journal of the Franklin Institute* 263(3): 195-206.

Rodríguez Jara, Enrique A., Sánchez de la Flor, Francisco J., Domínguez, Servando Álvarez, Félix, José L. Molina and Lissén, José M. Salmerón (2016). A new analytical approach for simplified thermal modelling of buildings: Self-Adjusting RC-network model. *Energy and Buildings* 130: 85-97.

Saberi Derakhtenjani, A. and Athienitis , A. K. (2016). A Study of the Effect of Zone Design Parameters on Frequency Domain Transfer Functions for Radiant and Convective Systems. *4th International High Performance Buildings Conference*, Purdue University, Westlafayette, IN.

Saberi Derakhtenjani, A., Candanedo, J, Chen, Y., Dehkordi, V and Athienitis , A. K. (2015). Modeling approaches for the characterization of building thermal dynamics and model-based control: A case study. *Science and Technology for the Built Environment* 21(6): 824-836.

Wang, Sh. and Xu, X. (2006). Parameter estimation of internal thermal mass of building dynamic models using genetic algorithm. *Energy Conversion & Management* 47: 1921-1941.

Xu, X. and Wang, Sh. (2007). Optimal simplified thermal models of building envelope based on frequency domain regression using genetic algorithm. *Energy and Buildings* 39(5): 525-536.